WORLD JOURNAL OF PHARMACEUTICAL RESEARCH
SJIF Impact Factor 8.084
Volume 10, Issue 10, 1170-1196. Research Article ISSN 2277– 7105

IN-VITRO TO IN-VIVO PREDICTION OF DRUG INTERACTIONS INVOLVING CYP3A TIME-DEPENDENT INACTIVATION

Snehal Prakash Agalave[1]*, Pranay Prabhakar Iskar[2] and Vishal Vijay Naik[3]

[1]Second Year B. Pharmacy of Shree Sarasvati Institute of Pharmacy, Tondavali, Kankavali, Sindhudurg, Maharashtra.

[2,3]Dr. Babasaheb Ambedkar Technological University, Lonere, Raigad, Maharashtra.

Article Received on
21 June 2021,

Revised on 11 July 2021,
Accepted on 01 August 2021

DOI: 10.20959/wjpr202110-21278

***Corresponding Author**
Snehal Prakash Agalave
Second Year B. Pharmacy of Shree Sarasvati Institute of Pharmacy, Tondavali, Kankavali,Sindhudurg, Maharashtra.

ABSTRACT

Time-dependent inactivation (TDI) of cytochrome P450s (CYPs) is a leading cause of clinical drug–drug interactions (DDIs). Current methods tend to overpredict DDIs. In this study, a numerical approach was used to model complex CYP3A TDI in human-liver microsomes. The inhibitors evaluated included troleandomycin (TAO), erythromycin (ERY), verapamil (VER), and diltiazem (DTZ) along with the primary metabolites N -dimethyl erythromycin (NDE), nor verapamil (NV), and N -dimethyl diltiazem (NDD). The complexities incorporated into the models included multiple-binding kinetics, quasi-irreversible inactivation, sequential metabolism, inhibitor depletion, and membrane partitioning. The resulting inactivation parameters were incorporated into static in vitro–in vivo correlation (IVIVC) models to predict clinical DDIs. For 77 clinically observed DDIs, with a hepatic-CYP3A-synthesis-rate constant of 0.000 146 min−1, the average difference between the observed and predicted DDIs was 3.17 for the standard replot method and 1.45 for the numerical method. Similar results were obtained using a synthesisrate constant of 0.000 32 min−1. These results suggest that numerical methods can successfully model complex in vitro TDI kinetics and that the resulting DDI predictions are more accurate than those obtained with the standard replot approach.

KEYWORDS: numerical method; time-dependent inhibition; drug–drug interactions; enzyme kinetic models.

INTRODUCTION

Drug–drug interactions (DDIs) can occur in patients undergoing polytherapy at pharmacokinetic (PK) and pharmacodynamic (PD) level, resulting in altered drug concentrations by either inhibiting or inducing the enzymes or transporters responsible for the disposition of that drug or producing agonistic or antagonistic effects.[1] Cytochrome P450s (CYPs) are an important superfamily of drug-metabolizing enzymes (DMEs) with 57 functional genes in humans.[1] These enzymes catalyze endogenous as well as xenobiotic metabolism. More than 90% of xenobiotics are metabolized by CYP1, −2, and −3 family members.[2] Cytochrome P450 enzymes (CYPs) are found in practically all living organisms and have been retained and adapted through evolution due to their unusual ability to oxidise carbon–hydrogen bonds in a regio- and stereo-selective manner. In addition to performing essential biosynthetic and metabolic functions (e.g. structural and signaling molecule biosynthesis, bacterial activation of hydrocarbons for use as carbon sources) animal P450 enzymes also act as important systems for the detoxification of phytochemicals and other xenobiotics. The human CYP enzymes which have evolved to dispose of a wide variety of dietary and environmental toxins now perform the same function in removal of lipophilic small molecule (molecular weight <1,200 Da) drug substances from the body.[4]

In time-dependent inhibition (TDI), the magnitude of inhibition increases as the contact time between the enzyme and inactivator increases. TDI is characterized by loss of activity with increases in time and concentration of the inactivator. There are several examples of drugs that demonstrate nonlinear accumulation and increased half-lives in humans after multiple doses because of enzyme inactivation. These include diltiazem (DTZ),[5] verapamil (VER), paroxetine(PAR), ticlopidine, and delavirdine.[6,7] Inactivation of CYPs can lead to drug–drug interactions (DDIs)[8–10] and adverse reactions,[11–16] which can result in the withdrawal of drugs from the market (e.g., mibefradil, cerivastatin, and soruvidines.

In Vitro TDI Incubations—Several CYP3A inactivators (DTZ, ERY, NDD, NDE, NV, TAO, and VER) were tested using a standard two-step approach for determining TDI inhibition of CYPs in the pooled HLM. MDZ was used as a probe substrate. Briefly, eight concentrations of inactivators with 2-fold dilution schemes (0–40 μ M DTZ, 0–50 μ M ERY, 0–10 μ M NDD, 0–50 μ M NDE, 0–40 μ M NV, 0–10 μ M TAO, and 0–40 μ M VER) were incubated at 37 °C in a 1 mg/mL suspension of HLM in 0.1 M potassium phosphate buffer (pH 7.4) as the primary incubation. After 5 min of preincubation, the reaction was initiated by the

addition of the NADPH-regenerating system (final concentrations of 1.3 mM NADP +, 3.3 mM glucose-6-phosphate, 0.4 U/mL glucose-6-phosphate dehydrogenase, and 3.3 mM magnesium chloride). At specific time points, aliquots (7.5 µ L) of the primary incubations were added to the secondary incubations (142.5 µ L), which contained 50 µ M MDZ and the NADPH- regenerating system (final concentrations of 1.3 mM NADP +, 3.3 mM glucose-6phosphate, 0.4 U/mL glucose-6-phosphate dehydrogenase, and 3.3 mM magnesium.

In Vitro: Reversible Inhibition

The potential for PF-00251802 and its metabolite PF-04015475 to reversibly inhibit human drug metabolizing enzymes in vitro was evaluated by determining half maximal inhibitory concentration (IC50) values. Pooled human liver microsomes were incubated with standard marker activity substrates (at concentrations near their determined Km values) and PF-00251802 (0–30 µM) or PF-04015475 (0–100 µM) in the presence of nicotinamide adenine dinucleotide phosphate (NADPH; 1.3 mM). Human liver microsome concentrations and times were chosen to respect thelinearityof the reaction for each probe substrate. At the end of the incubation period, termination solvent containing internal standard was added and the incubation mixture filtered to remove microsomal protein.

In Vitro: Time-Dependent Inhibition

The potential for PF-00251802 and PF-04015475 to produce time-dependent inhibition of CYPs in vitro was determined using midazolam (PF-00251802 and PF-04015475) and dextromethorphan (PF00251802 only) as marker substrates for CYP3A and CYP2D6, respectively. Pooledhumanlivermicrosomes (0.3 mg/mL) were incubated with NADPH (1.3 mM) and PF-00251802 (0.03–5 µM) for 1, 2, 4, 6, 13, and 20 minutes (midazolam assay) or 1, 5, 10, 21, 30, and 41 minutes (dextromethorphan assay) or PF-04015475 (0.3–30 µM) for 1, 5, 10, 20, 30, and 40 minutes (midazolam assay). An aliquot of the primary incubation mixture was then added to a secondary reaction containing NADPH(1.3mM)and midazolam (23 µM) or dextromethorphan (14.4 µM), resulting in a 20-fold dilution from the primary incubation to minimize reversible inhibition of each investigational agent on CYP enzymes. Following a 6-minute (midazolam assay) or 10-minute (dextromethorphan assay) incubation, the reaction was terminated, and samples were analyzed using HPLC-MS/MS for formation of 1-hydroxymidazolam or dextrorphanol. Data were analyzed using the procedure for time dependent inhibition of CYP enzymes described by Yates et al (2012).

Characteristics of Human Cyp3a

Tissue Localization A considerable amount of information exists on the characteristics of the members in the CYP3A subfamily of enzymes in both animals and humans (1). At least three functional proteins exist in humans. CYP3A4 is universally found in the liver, where it constitutes the major isoform—on average about 30% of total CYP protein (2). Relatively high CYP3A4 levels—about 50% of hepatic levels and 70% of total CYP protein—are also present in small intestinal epithelium, particularly in the apical region of mature enterocytes at the tip of the microvillus (3,4). The amount of isoform progressively falls along the remainder of the gastrointestinal tract. In the kidney, however, CYP3A4 is present in only about 30% of renal tissue samples, mainly in the collecting ducts (5,6); the mechanism for such polymorphic expression is not currently understood. CYP3A3 is a very closely related isoform to CYP3A4 (>98% cDNA sequence similarity), but it is not known whether this reflects a separate gene product or an allelic variant. Therefore, the term CYP3A4 is generally taken to indicate.

Measurement of Cyp3a Activity In Vitro

In vitro approaches to studying CYP3A activity have the advantage that condition scan be more closely controlled and altered than in vivo. On the other hand, the selected conditions may not sufficiently reflect those present in vivo, and experimental findings cannot be readily extrapolated, especially in a quantitative fashion. This is particularly true as the level of cellular integrity and organization decreases. Nevertheless, valuable information concerning many aspects of CYP- mediated metabolism applicable to drug development and clinical use has been obtained using a variety of different preparations Microsomal Partitioning and Human-Plasma-Protein Binding—Equilibrium dialysis was performed to determine the microsomal partitioning of all the inactivators except TAO in HLM and human plasma. For TAO, the unbound fractions in HLM (f u,mic) and human plasma (f u,p) reported in the literature were used.36,37 Briefly, 0.5 mg/mL HLM suspensions were spiked with DTZ, ERY, NDD, NDE, NV, and VER at final concentrations of 2 μ M in separate experiments (n = 5 replicates). The unbound fractions in plasma were determined for the parent inactivators only (DTZ, ERY, and VER) using a similar approach. A 96-well equilibrium dialyzer (Harvard Apparatus) was used to perform the dialyses with inactivator-spiked HLM suspensions or human plasma on one side and blank phosphate buffer (pH 7.4) on the other side at 37 °C for 20 h with 5% CO2. The samples on each side of the membrane were analyzed by LC-MS/MS for inactivator concentrations. The unbound fractions (f u) were

calculated by using the following equation.

$$f_u = \frac{C_{buffer}}{C_{matrix}} \quad (1)$$

where f u, C matrix, and C buffer represent the unbound fraction, the total concentration in the matrix (either the HLM suspension or human plasma), and the total concentration in the phosphate buffer, respectively. The f u,mic value was scaled to 1 mg/mL using the equation.[38]

$$f_{u,mic(1mg/mL)} = \frac{\frac{1}{D}}{\left(\frac{1}{f_{u,mic(1mg/mL)}} - 1\right) + \frac{1}{D}} \quad (2)$$

where f u,mic(1mg/mL) is the scaled unbound fraction at 1 mg/mL microsomal protein, and f u,mic(0.5mg/mL) is the unbound fraction experimentally measured at 0.5 mg/mL. D = 2 is the dilution factor.

In Vitro TDI Model Development

The concentrations of 1-OH MDZ obtained from the in vitro TDI experiments were converted to logarithmic percent-remaining-activity plots (PRA plots) and further evaluated for model development. All the inactivators evaluated in this study are known to be MIC-forming compounds[39–42] by quasi-irreversible mechanisms. On the basis of the reported mechanism of inactivation[34] and the data sets generated, kinetic models for CYP3A TDI were developed. Concave upward curvature is indicative of either quasi- irreversible or partial inactivation, as shown previously.[32] Using the numerical method,[32,33] the kinetic models were fit to the data, and the kinetic parameters were estimated. The initial estimates of the rate constants were obtained from analyzing the data as detailed in previous publications.[32–34] Briefly, nonspecific loss of enzyme activity was incorporated into the model if activity loss over time was observed in the absence of inactivators (0 μ M inactivator). The initial estimate for the rate constant for nonspecific enzyme loss (k 9) was obtained by fitting a first-order degradation model to the 0 μ M inactivator data. All the active enzyme species were assumed to degrade with first-order kinetics. Furthermore, a competitive-inhibition model was fit to the 0- and 60-min time point data to obtain an initial estimate for K I. A difference in the initial estimate of K I from the 0 min data versus that from the 60 min data was indicative of multiple binding. As shown previously,[34] MIC formation is a complex multistep process involving the formation of Fe3+: carbene and Fe2+:

carbene. Hence, enzyme inactivation was modeled with three types of rate constants. For example, in Figure 1A, k 6 and k 12were used for Fe3+: carbene formation, k 7 was used for the reformation of the active enzyme, and k 8 was used for Fe2+:carbene formation The association-rate constants (k 1, k 4, and k 10) were fixed at 270 μ M−1 min−1, and initial estimates for the dissociation-rate constants were obtained from the data.34 For MDZ, the association- (k 1) and dissociation-rate constants (k 2) were fixed at 270 μ M−1 min−1 and 1350 min−1, respectively (assuming a K m of 5 μ M). Lipid partitioning was also incorporated into the models to account for microsomal partitioning. The association- rate constant for the lipids was set at 2000 μ M−1 min−1, and the dissociation-rate constant was calculated using the followingequation.[45]

$$k_{off} = \frac{f_{u,mic} k_{on}}{1 - f_{u,mic}} \quad (3)$$

where k on is the association-rate constant, k off is the dissociation- rate constant, and f u,mic is the unbound fraction in the microsomes The K I values were estimated from the ratios of the association- and dissociation-rate constants (assuming rapid equilibrium). The K I obtained from the numerical method is the same as the unbound one, K I,u (i.e., K I,u = K I), because lipid partitioning was incorporated into the model. The inactivation parameters (k in act) were calculated using the partition method as described previously;46 for example, for the scheme in Figure 2, k in act can be calculated as a net rate constant.

$$k_{inact} = \frac{1}{\frac{1}{k_8} + \frac{k_8 + k_7}{k_6 k_8}} \quad (4)$$

For TAO (e.g., see Figure 1) and NV, k in act was described as

$$k_{inact} = \frac{1}{\left(\frac{1}{k'_6} + \frac{1}{k_8} + \frac{k'_{10}}{k'_6 k'_{12}} + \frac{1}{k'_{10}} + \frac{1}{k'_{12}} + \frac{1}{k_8} + \frac{k'_6}{k'_{10}}\right)} \quad (5)$$

where

$$k'_6 = \frac{k_6 k_8}{k_7 + k_8}$$

$$k'_{10} = \frac{k_{10} k'_{12}}{k_{10} + k'_{12}}$$

$$k'_{12} = \frac{k_{10} k_8}{k_7 + k_8}$$

The parameter errors for net rate constants were calculated with error propagation for individual rate constants. AICc47 and adjusted R 2 were used to compare the different models for each data set.

The replot method22 was also used to analyze the in vitro TDI data sets. The data were analyzed either by using all the data (data not shown) or only the linear parts of the PRA plots.22 The following replot equation was used to obtain the estimates of K I and k in act.

$$k_{obs} = \frac{k_{inact}[I]}{K_I + [I]} \quad (6)$$

For the comparison with the numerical method, the K I obtained from the replot method was corrected for microsomal partitioning by multiplying K I with f u,mic to obtain K I,u. Model fitting was conducted with Mathematica 11.0.1.0 (Wolfram Research). The Nonlinear Model Fit function was used to fit the model to the data with a Precision Goal of 10, finite difference derivatives of an order of 4, and 1/ Y weighting. The When Event function was used to incorporate the dilution step in the model.

In Vitro–In Vivo Correlation (IVIVC)—DDI predictions using K I,u and k in act obtained from either the replot or numerical method were performed using the following static equations.37 Equation 7 was used when the probe substrate was dosed through an intravenous route, and eq 8 was used when probe substrate was dosed orally.

$$\frac{AUC_i}{AUC} = \left(\frac{1}{\left(\frac{k_{deg,h}}{k_{deg,h} + \left(\frac{[I]_h k_{inact}}{[I]_h + k_I} \right)} \right) f_{m,CYP3A} + \left(1 - f_{m,CYP3A}\right)} \right) \quad (7)$$

$$\frac{AUC_i}{AUC} = \left(\frac{1}{F_g + \left(1 - F_g\right) \left(\frac{k_{deg,g}}{k_{deg,g} + \left(\frac{[I]_g k_{inact}}{[I]_g + k_I} \right)} \right)} \right) \quad (8)$$

$$\times \left(\frac{1}{\left(\frac{k_{deg,h}}{k_{deg,h} + \left(\frac{[I]_h k_{inact}}{[I]_h + k_I} \right)} \right) f_{m,CYP3A} + \left(1 - f_{m,CYP3A}\right)} \right)$$

where AUCi and AUC are the areas under the plasma- concentration–time curves of the probe substrates in the presence and absence of the inactivator, respectively; f m,CYP3A is the fraction of MDZ metabolized by CYP3A; F g is the fraction that escapes gut metabolism (Table 1); [I]h and [I]g are the inactivator concentrations in hepatic portal vein and gut, respectively; and k deg,h and k deg,g are the degradation-rate constants of hepatic (0.000 146 min−1)[48] and gut (0.000 481 min−1)[49] CYP3A, respectively. It was assumed that K I and k inact were equivalent for hepatic and gut enzymes. Different values were used for in vivo inactivator concentrations depending on the clinical-DDI-study design. In cases where the

victim drug was given orally, [I]h,u and [I]g,u were used for the in vivo inhibitor concentrations, as given by the following equations.[50]

$$[I]_h = \left([I]_{max} + \frac{Dk_a F_a F_g}{Q_h BP}\right) \quad (9)$$

$$[I]_{h,u} = f_{u,g}[I]_h \quad (10)$$

$$[I]_{g,u} = f_{u,g}\left(\frac{DK_a F_a}{Q_g}\right) \quad (11)$$

where [I]max is the maximum concentration of the inactivator in the plasma after an oral dose; D is the dose; F a is the fraction absorbed; k a is the first-order absorption-rate constant; Q g (0.3 L/min)and Q h (1.5 L/min) are the gut and hepatic blood flows, respectively; f u,p is the unbound fraction in the plasma; f u,g (assumed to be equal to 1) is the unbound fraction in the enterocytes; and BP is the blood-to-plasma-partition ratio. In cases where the victim drug was administered intravenously, the maximum unbound concentration, [I]max,u, was used as the inactivator concentration for the DDI prediction. [I] max,u was given by the following equation.[51]

$$[I]_{max,u} = f_{u,p}\frac{[I]_{sys} k\tau}{1 - e^{-k\tau}} \quad (12)$$

where τ is the dosing interval, and k is the elimination-rate constant, which is calculated by the following equation.

$$k = \frac{CL_s}{V_{ss}} \quad (13)$$

where CLs is the systemic clearance, and V so is the volume of distribution at steady state. [I]sys is the average systemic inactivator concentration.

$$[I]_{sys} = \frac{FD}{\tau CL_s} \quad (14)$$

where F is the bioavailability.

[I]sys,u was calculated using the following equation.

$$[I]_{sys,u} = [I]_{sys} f_{u,p} \quad (15)$$

The values reported in the literature for the substrate-dependent parameters (F g and f m,CYP3A) are listed in Table 1. F g and f m,CYP3A values were calculated for substrates for which literature values were not available. The inactivator pharmacokinetic (PK) parameters.

RESULTS

In Vitro TDI Models

Several kinetic models were developed for each inactivator depending upon the reported mechanism of inactivation and the observed data set. A best-fit model for each inactivator was chosen on the basis of the AICc values. In those cases (e.g., DTZ and VER) where multiple models resulted in equally good fits (based on AICc), all the best-fit models were reported.

For TAO, because there was no activity loss observed in the 0 μ M incubation, enzyme loss was not incorporated into the model. The observed PRA plots show concave upward curvature, suggesting either quasi-irreversible or partial inactivation (Figure 1). Analysis of the observed PRA plots shows that the different TAO concentrations plateau at different levels, indicating quasi-irreversible mechanisms rather than partial inactivation.32 An MIC model with EII formation (MIC-EII-IL) provided the best fit. The concave upward curvature observed even at the highest inhibitor concentration indicates that inhibitor depletion is not the cause of the curvature in the PRA plots. An MIC-EII-IL model with an inhibitor-depletion step did not converge unless the inhibitor-depletion-rate constant was fixed at <0.001 min−1 (data not shown), suggesting minimal inhibitor loss. Estimates of K I,u and k inact from the numerical and replot methods for TAO are shown in Table 3. Our experimental replot parameters agree with the literature values (see the Supporting Information, Table S6). The numerical method yields a 3.02-fold lower inactivation efficiency (k inact/ K I,u) for TAO than that from the replot method.

For the other inactivators (ERY, DTZ, and VER), TDI was also evaluated for their primary

metabolites (NDE for ERY, NDD for DTZ, and NV for VER). The primary metabolites of TAO were not available commercially and were not evaluated. When sequential metabolism was considered, the model for the metabolite was first constructed. This model was then incorporated into the parent TDI model.

In Vitro–In Vivo Correlation (IVIVC)

The DDI predictions were performed using the standard static model as recommended by the FDA.52 Because there is a wide range of k deg,h values reported in the literature,48,49,53–58 three different values for k deg, h (ranging from 0.0004 to 0.000 082 5 min−1) were used for the DDI predictions. The results for two k deg,h values (k deg,h = 0.000 146 min−1, an average of the reported values, and k deg,h = 0.000 32 min−1, a commonly used value in the literature) are listed in Table 6. In the cases of VER and DTZ, DDI predictions were performed only using the K I1,u and k inact from the simplest of the three models. The DDI predictions using the K I,u and k inact from the replot method were higher than those using the K I,u and k inact from the numerical method. The average fold differences between the observed and predicted values were 3.64 for the replot method and 1.41 for the numerical method when a hepatic k deg value of 0.000 146 min−1 was used. The average fold differences between the observed and predicted values were 2.8 for the replot method and 0.95 for the numerical method when a hepatic k deg value of 0.0003 min−1 was used.

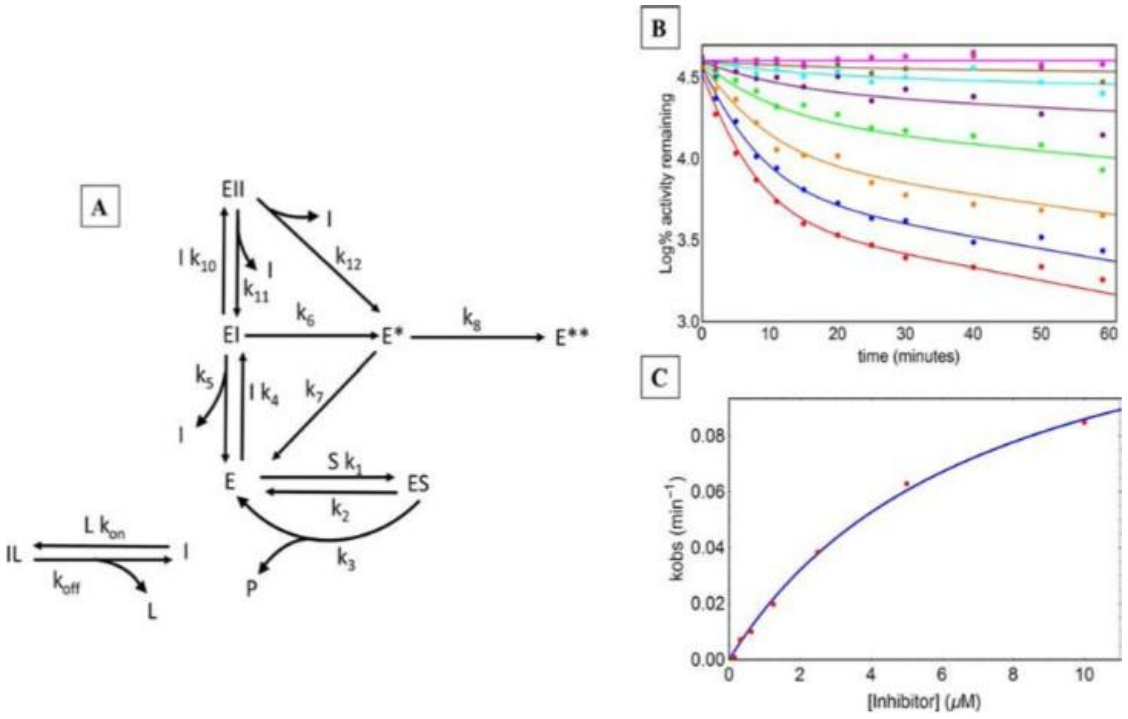

Figure 1.

Kinetic scheme for CYP3A inhibition by TAO (10, 5, 2.5, 1.25, 0.625, 0.313, 0.156, and 0 μM) in HLM. (A) Kinetic scheme for the MIC-EII-IL model. E, enzyme; I, inhibitor; L, lipid; P, product; S, substrate; k, rate constant.

(B) Experimental (points) and MIC-EII-IL- model-fitted (solid lines) PRA plots. (C) Plot of k_{obs} vs [I] for thestandard replot method with linear data points (n = 4 points).

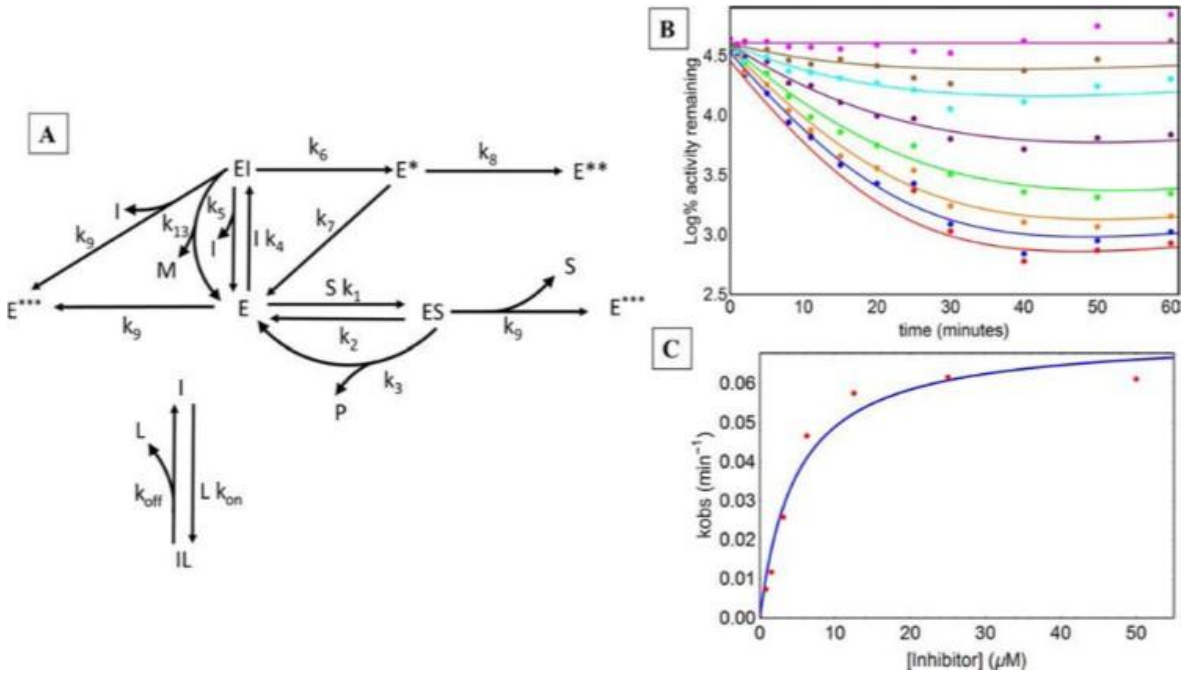

Figure 2.

Kinetic scheme for CYP3A inhibition by NDE (50, 25, 12.5, 6.25, 3.13, 1.56, 0.78, and 0 μM) in HLM. (A) Kinetic scheme for the MIC-IL-M model. E, enzyme; I, inhibitor; L, lipid; M, inhibitor metabolite; P, product; S, substrate; k, rate constant. (B) Experimental (points) and MIC-IL-M-model-fitted (solid lines) PRA plots. (C) Plot of k_{obs} vs [I] for the standard replot method with linear data points (n = 4 points).

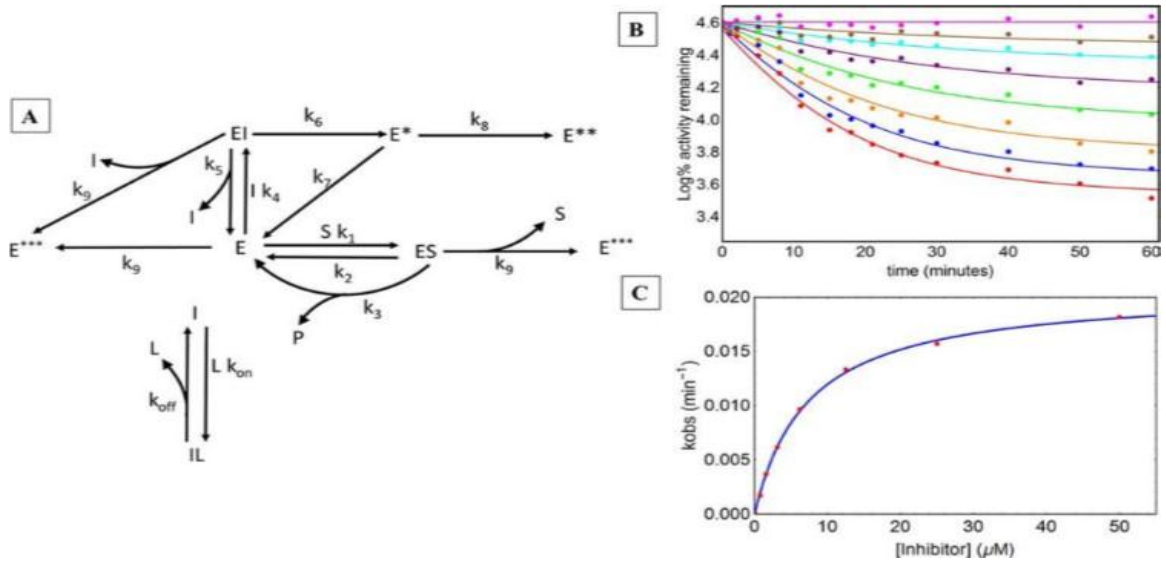

Figure 3.

Kinetic scheme for CYP3A inhibition by ERY (50, 25, 12.5, 6.25, 3.13, 1.56, 0.78, and 0 μM) in HLM. (A) Kinetic scheme for the MIC-IL model. E, enzyme; I, inhibitor; L, lipid; P, product; S, substrate; k, rate constant. (B) Experimental (points) and MIC-IL-model-fitted (solid lines) PRA plots. (C) Plot of k_{obs} vs [I] for the standard replot method with linear data points (n = 7 points).

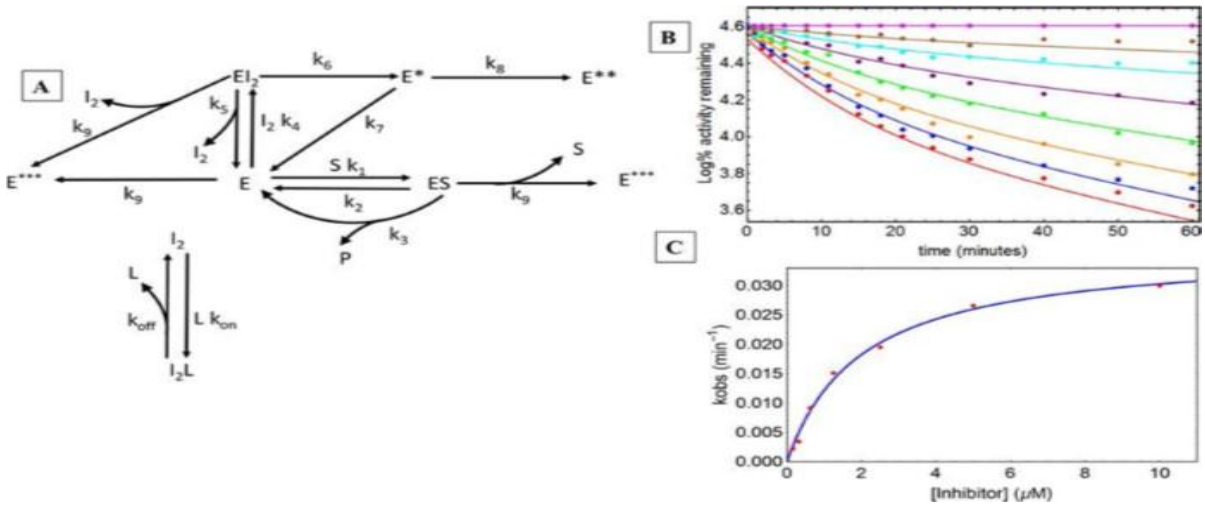

Figure 4.

Kinetic scheme for CYP3A inhibition by NDD (10, 5, 2.5, 1.25, 0.625, 0.313, 0.156, and 0 μM) in HLM. (A) Kinetic scheme for the MIC-I_2L model. E, enzyme; I_2, metabolite inhibitor; L, lipid; P, product; S, substrate; k, rate constant. (B) Experimental (points) and MIC-I_2L-model-fitted (solid lines) PRA plots. (C) Plot of k_{obs} vs [I] for the standard replot method with linear data points (n = 7 points).

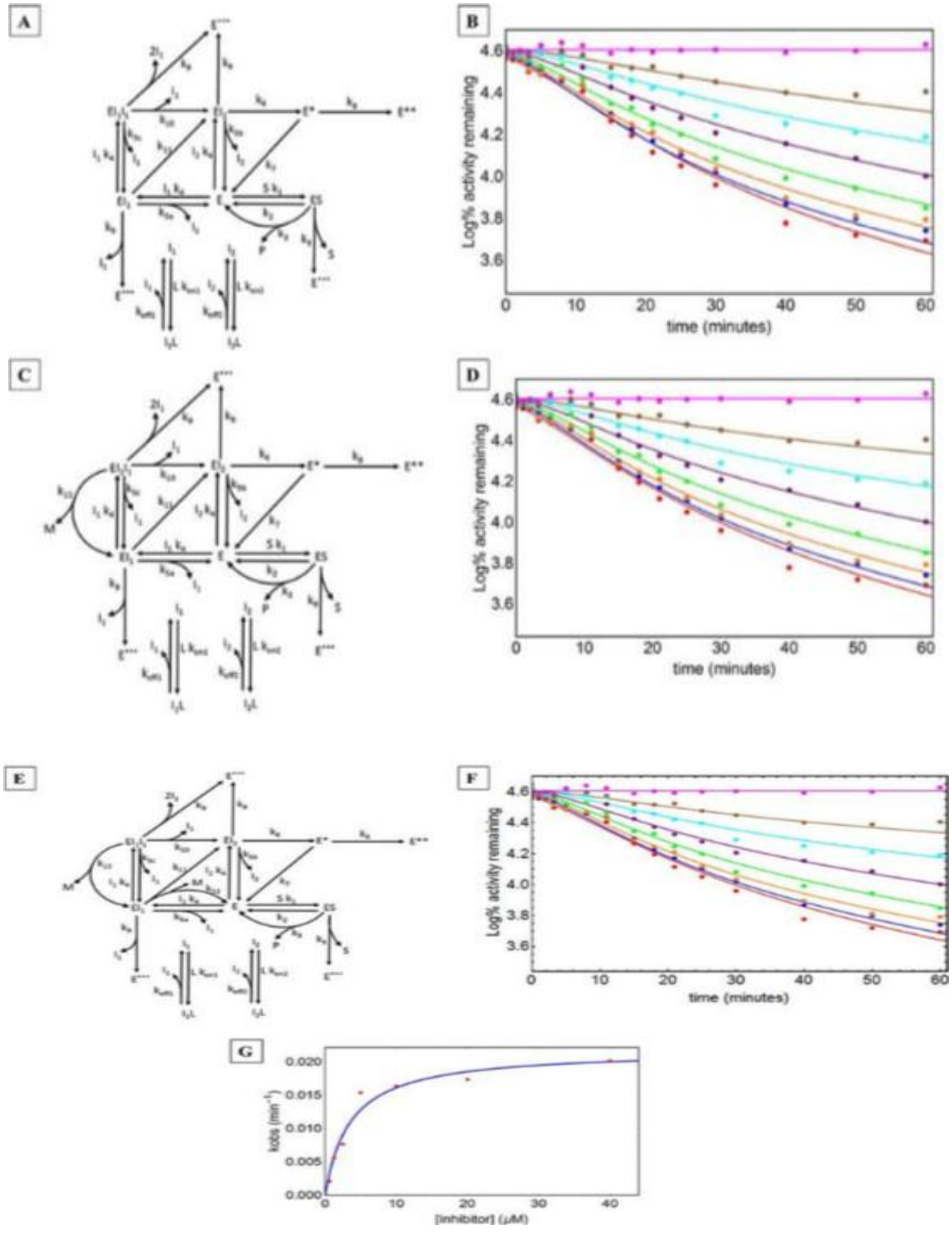

Figure 5.

Kinetic schemes for CYP3A inhibition by DTZ (40, 20, 10, 5, 2.5, 1.25, 0.625, and 0 μM) in HLM. (A) Kinetic scheme for the Seq-MIC-EI$_1$I$_1$- I$_1$L-I$_2$L model. (B) Experimental (points) and Seq-MIC-EI$_1$I$_1$-I$_1$L-I$_2$L-model-fitted(solid lines) PRA plots. (C) Kinetic scheme for the

Seq-MIC-EI$_1$I$_1$- M-I$_1$L-I$_2$L model. (D) Experimental (points) and Seq-MIC-EI$_1$I$_1$-M-I$_1$L-I$_2$L-model-fitted (solid lines) PRA plots. (E) Kinetic scheme for the Seq-MIC- EI$_1$I$_1$- MM-I$_1$L-I$_2$L model. (F) Experimental (points) and Seq-MIC-EI$_1$I$_1$-MM-I$_1$L-I$_2$L-model-fitted (solid lines) PRA plots. (G) Plot of k_{obs} vs [I] for the standard replot method with linear data.

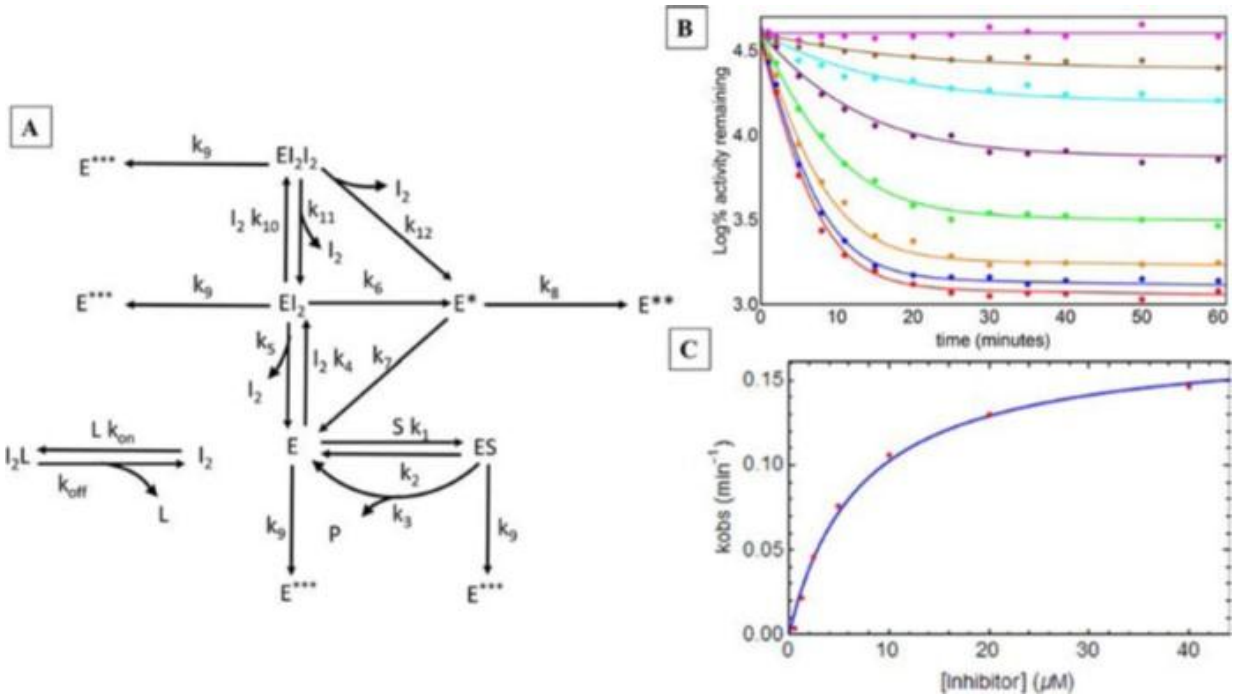

Figure 6.

Kinetic scheme for CYP3A inhibition by NV (40, 20, 10, 5, 2.5, 1.25, 0.625, and 0 μM) in HLM. (A) Kinetic scheme for the MIC-EI$_2$I$_2$-I$_2$L model. E, enzyme; I$_2$, metabolite inhibitor; L, lipid; P, product; S, substrate; k, rate constant. (B) Experimental (points) and MIC-EI$_2$I$_2$-I$_2$L-model-fitted (solid lines) PRA plots. (C) Plot of k_{obs} vs [I] for the standard replot method with linear data points (n = 4 points).

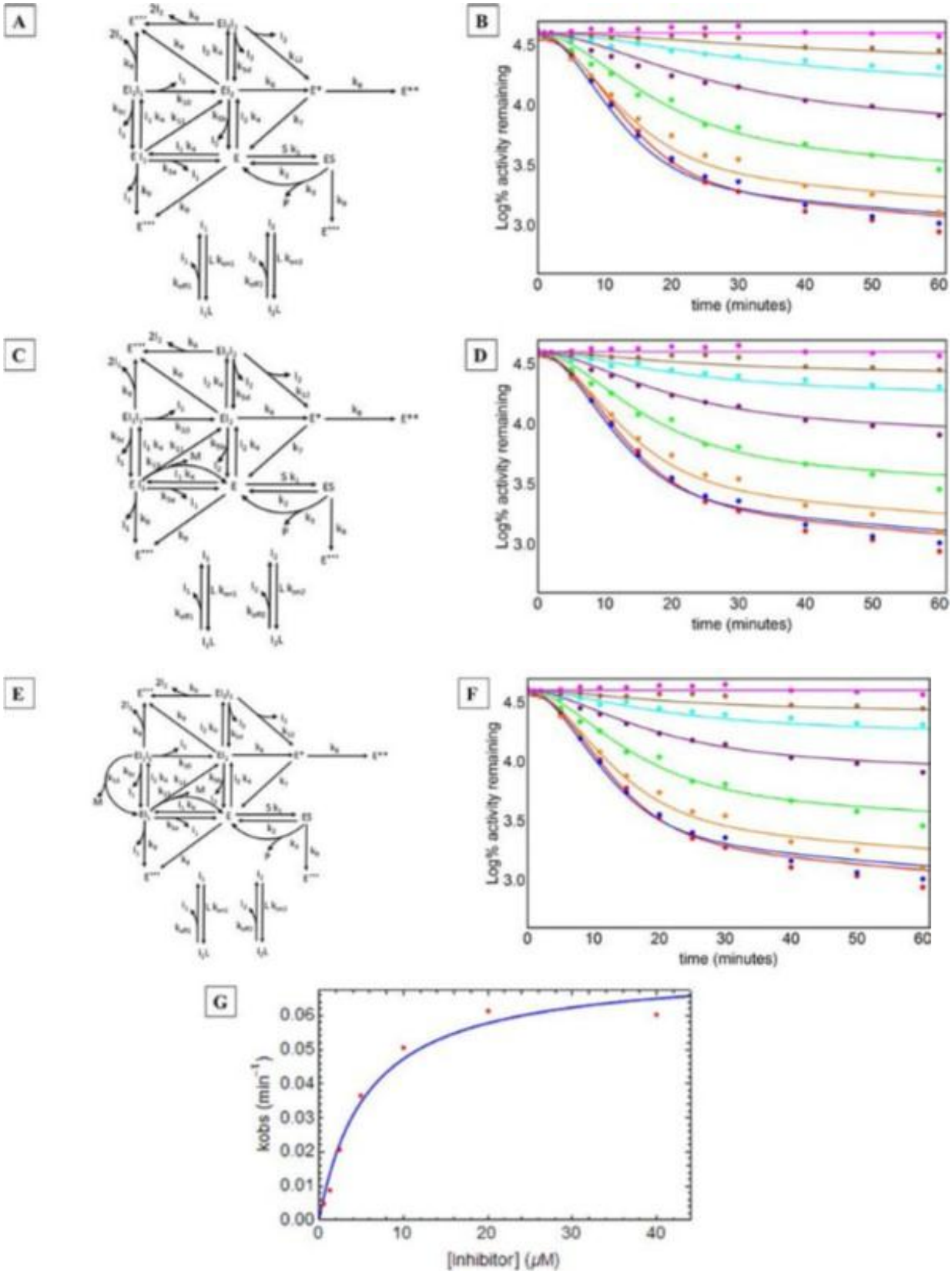

Figure 7.

Kinetic schemes for CYP3A inhibition by VER (40, 20, 10, 5, 2.5, 1.25, 0.625, and 0 μM) in HLM. (A) Kinetic scheme for the Seq-MIC-EI$_1$I$_1$-EI$_2$I$_2$-I$_1$L-I$_2$L model. (B) Experimental

(points) and Seq-MIC-EI$_1$I$_1$-EI$_2$I$_2$-I$_1$L-I$_2$L- model-fitted (solid lines) PRA plots. (C) Kinetic scheme for the Seq- MIC-EI$_1$I$_1$-EI$_2$I$_2$-M-I$_1$L-I$_2$L model. (D) Experimental (points) and Seq-MIC-EI$_1$I$_1$-EI$_2$I$_2$-M-I$_1$L-I$_2$L-model-fitted (solid lines) PRA plots. (E) Kinetic scheme for the Seq-MIC-EI$_1$I$_1$-EI$_2$I$_2$-MM-I$_1$L-I$_2$L model. (F) Experimental (points) and Seq-MIC-EI$_1$I$_1$- EI$_2$I$_2$-MM- I$_1$L-I$_2$L-model-fitted (solid lines) PRA plots. (G) Plot of k_{obs} vs [I] for the.

ABBREVIATIONS

CYPs cytochromes P450 DDI drug–drug interactions

DME – drug-metabolizing enzymesDTZ- diltiazem

ERY- erythromycin

HLM- human liver microsomes IVIVC- in vitro–in vivo correlationTAO- troleandomycin

TDI- time-dependent inhibition

REFERENCES

1. Zhou Z-W, Zhou S-F. Application of mechanism-based CYP inhibition for predicting drug–drug interactions. Expert Open Drug Metal Toxically, 2009; 5(6): 579–605. [PubMed: 19466877]
2. Nebert DW, Russell DW. Clinical importance of the cytochromes P450. Lancet, 2002; 360(9340): 1155–1162. [PubMed: 12387968]
3. Zhou S, Chan E, Lim LY, Boelsterli UA, Li SC, Wang J, Zhang Q, Huang M, Xu A. Therapeutic drugs that behave as mechanism-based inhibitors of cytochrome P450 3A4. Curr Drug Metab, 2004; 5(5): 415–442. [PubMed: 15544435]
4. Fontana E, Dansette P, Poli S. Cytochrome p450 enzymes mechanism-based inhibitors: common sub-structures and reactivity. Curr Drug Metab, 2005; 6(5): 413–451. [PubMed: 16248836]
5. Tsao S, Dickinson T, Abernethy D. Metabolite inhibition of parent drug biotransformation. Studies of diltiazem. Drug Metab Dispos, 1990; 18(2): 180–182. [PubMed: 1971570]
6. Venkatakrishnan K, Obach RS. Drug-drug interactions via mechanism-based cytochrome P450 inactivation: points to consider for risk assessment from in vitro data and clinical pharmacologic evaluation. Curr Drug Metab, 2007; 8(5): 449–462. [PubMed: 17584016]
7. Cheng C-L, Smith DE, Carver PL, Cox SR, Watkins PB, Blake DS, Kauffman CA, Meyer KM, Amidon GL, Stetson PL. Steady-state pharmacokinetics of delavirdine in

HIV-positive patients: effect on erythromycin breath test. Clin Pharmacol Ther. 1997; 61: 531–543. [PubMed: 9164415]

8. Watanabe A, Nakamura K, Okudaira N, Okazaki O, Sudo K-I. Risk assessment for drug-drug interaction caused by metabolism-based inhibition of CYP3A using automated in vitro assay systems and its application in the early drug discovery process. Drug metabolism and disposition, 2007; 35(7): 1232–1238. [PubMed: 17392390]
9. Zhou S-F, Xue CC, Yu X-Q, Li C, Wang G. Clinically important drug interactions potentially involving mechanism-based inhibition of cytochrome P450 3A4 and the role of therapeutic drug monitoring. Ther Drug Monit, 2007; 29(6): 687–710. [PubMed: 18043468]
10. Backman JT, Olkkola KT, Aranko K, Himberg J-J, Neuvonen PJ. Dose of midazolam should be reduced during diltiazem and verapamil treatments. British journal of clinical pharmacology, 1994; 37(3): 221–225. [PubMed: 8198928]
11. Michalets EL, Williams CR. Drug interactions with cisapride. Clin Pharmacokinet, 2000; 39(1): 49–75. [PubMed: 10926350]
12. Mullins ME, Horowitz BZ, Linden DH, Smith GW, Norton RL, Stump J. Life-threatening interaction of mibefradil and β -blockers with dihydropyridine calcium channel blockers. JAMA, 1998; 280(2): 157–158. [PubMed: 9669789].
13. GuengerichFP.1995.Humancytochrome P450 enzymes. In Cytochrome P450: Structure, Mechanism, and Biochemistry, ed. PR Ortiz de Montellano, pp. 473–535. New York: Plenum.
14. Aoyama T, Yamano S, Waxman DJ, Lapenson DP, Meyer UA, et al. 1989. Cytochrome P-450 hPCN3, a novel cytochrome P-450 IIIA gene product that is differentially expressed in adult human liver. cDNA and deduced amino acid sequence and distinct specific it is of DNA expressed hPCN1 and hPCN3 for the metabolism of steroid hormones and cyclosporine. J. Biol. Chem, 264: 10388–95.
15. Gorski JC, Hall SD, Jones DR, Vandenbranden M, Wrighton SA. 1994. Regioselective biotransformation of midazolam by members of the human cytochrome P450 3A (CYP3A) subfamily. Biochem. Pharmacol, 47: 1643–53.
16. Lown KS, Kolars JC, Thummel KE, Barnett JL, Kunze KL, et al. 1994. Interpatient heterogeneity in expression of CYP3A4 and CYP3A5 in small bowel— lack of prediction by the erythromycin breath test. Drug Metab. Disp, 22: 947–55 17.
17. Gottesman MM, Pastan I. 1993. Biochemistry of multidrug resistance mediated by the multidrug transporter. Annu. Rev. Biochem, 62: 385–427.

18. Fahmi OA, Hurst S, Plowchalk D, et al. Comparison of different algorithms for predicting clinical drug-drug interactions, based on the use of CYP3A4 in vitro data: predictions of compounds as precipitants of interaction. Drug Metab Dispos, 2009; 37(8): 1658–1666.
19. Vieira ML, Kirby B, Ragueneau-Majlessi I, et al. Evaluation of various static in vitro-in vivo extrapolation models for risk assessment of the CYP3A inhibition potential of an investigational drug. Clin Pharmacol Ther, 2014; 95(2): 189–198.
20. Fahmi OA, Maurer TS, Kish M, Cardenas E, Boldt S, Nettleton D. A combined model for predicting CYP3A4clinical net drug-drug interaction based on CYP3A4 inhibition, inactivation, and induction determined in vitro. Drug Metab Dispos, 2008; 36(8): 1698–1708.
21. Wang YH. Confidence assessment of the Simcyp time-based approach and a static mathematical model in predicting clinical drug-drug interactions for mechanism-based CYP3A inhibitors. Drug Metab Dispos, 2010; 38(7): 1094–1104.
22. Rowland Yeo K, Walsky RL, Jamei M, RostamiHodjegan A, Tucker GT. Prediction of time- dependent CYP3A4drug-druginteractionsbyphysiologicallybased pharmacokinetic modelling: impact of inactivation parameters and enzyme turnover. Eur J Pharm Sci, 2011; 43(3): 160–173.
23. Weatherley B, McFadyen L, Conrado D, Tammara B. The Population Pharmacokinetics of Active Metabolites of a prodrug PF-0417132, (Dissociated Agonist of Glucocorticoid Receptor), in Rheumatoid Arthritis subjects [abstract]. Abstract presented at PAGE 24. 2015. www page-meeting org/default asp?abstract = 3381.
24. Haupt LJ, Kazmi F, Ogilvie BW, et al. The reliability of estimating Ki Values for direct, reversible inhibition of cytochrome P450 enzymes from corresponding IC50 values: a retrospective analysis of343 experiments. Drug Metab Dispos, 2015; 43(11): 1744–1750.
25. Venkatakrishnan K, Obach RS. In vitro-in vivo extrapolation of CYP2D6 inactivation by paroxetine: prediction of nonstationary pharmacokinetics and drug interaction magnitude. Drug Metab Dispos, 2005; 33(6): 845–852.
26. Stock T, Fleishaker D, Wang X, Mukherjee A, Mebus C. Improved disease activity with fosdagrocorat (PF04171327), a partial agonist of the glucocorticoid receptor, in patients with rheumatoid arthritis: a phase 2 randomized study. Int J Rheum Dis, 2017; 20(8): 960– 970.
27. Varma, M.V.; Pang, K.S.; Isoherranen, N.; Zhao, P.Dealingwiththecomplexdrug-druginteractions: Towards mechanistic models. Bio pharm. Drug Dispos, 2015; 36: 71–92. [CrossRef] [PubMed]

28. Zanger, U.M.; Schwab, M. Cytochrome P450 enzymes in drug metabolism: Regulation of gene expression, enzyme activities, and impact of genetic variation. Pharmacol. Ther, 2013; 138: 103–141. [CrossRef]
28. In Vitro Drug Interaction Studies—Cytochrome P450 Enzymes- and Transporter-Mediated Drug Interactions Guidance for Industry. Available online: https: //www.fda.gov/regulatory- information/search-fda-guidance-documents/vitro-drug-interactionstudies-cytochrome-p450- enzyme-and-transporter-mediated-drug-interactions (accessed on 3 December 2020).
29. Giacomini, K.M.; Huang, S.M.; Tweedie, D.J.; Benet, L.Z.; Brouwer, K.L.; Chu, X.; Dahlin, A.; Evers, R.; Fischer, V.; Hillgren, K.M.; et al. Membrane transporters in drug development. Nat. Rev. Drug Discover, 2010; 9: 215–236.
30. Varma,M.V.; Gardner,I.; Steyn,S.J.; Nkansah,P.; Rotter,C.J.; WhitneyPickett,C.; Zhang,H.; Di,L.; Cram,M.; Fennerm, K.S.; et al. pH-Dependent solubility and permeability criteria for provisional biopharmaceutics classification (BCS and BDDCS) in early drug discovery. Mol. Pharm, 2012; 9:1199–1212. [CrossRef]
31. Yu, J.; Zhou, Z.; Tay-Sontheimer, J.; Levy, R.H.; Ragueneau-Majlessi, I. Risk of Clinically Relevant Pharmacokinetic-Based Drug-Drug Interactions with Drugs Approved by the U.S. Food and Drug Administration Between 2013 and 2016. Drug Metab. Dispos, 2018; 46: 835–845. [CrossRef]
32. Tachibana, T.; Kato, M.; Takano, J.; Sugiyama, Y. Predicting drug-drug interactions involving the inhibition of intestinal CYP3A4 and P-glycoprotein. Curr. Drug Metab, 2010; 11: 762–777. [CrossRef]
33. Fenner, K.S.; Troutman, M.D.; Kempshall, S.; Cook, J.A.; Ware, J.A.; Smith, D.A.; Lee, C.A. Drug- drug interactions mediated through P-glycoprotein: Clinical relevance and in vitro-in vivo correlation using digoxin as a probe drug. Clin. Pharmacol. Ther, 2009, 85, 173–181. [CrossRef]
34. Barnaba C, Yadav J, Nagar S, Korzekwa K, Jones JP. Mechanism-Based Inhibition of CYP3A4 by Podophyllotoxin: Aging of an Intermediate Is Important for in Vitro/in Vivo Correlations. Mol Pharmaceutics, 2016; 13(8): 2833–2843.
35. Pham C, Nagar S, Korzekwa K. Numerical analysis of time dependent inhibition kinetics: comparison between rat liver microsomes and rat hepatocyte data for mechanistic model fitting. Xenobiotica, 2017; in press. doi: 10.1080/00498254.2017.1345020
36. Zhao P, Kunze KL, Lee CA. Evaluation of time-dependent inactivation of CYP3A in cryopreserved human hepatocytes. Drug Metab Dispos, 2005; 33(6): 853–861.

[PubMed: 15743977]

37. Fahmi OA, Hurst S, Plowchalk D, Cook J, Guo F, Youdim K, Dickins M, Phipps A, Darekar A, Hyland R, et al. Comparison of different algorithms for predicting clinical drug-drug interactions, based on the use of CYP3A4 in vitro data: predictions of compounds as precipitants of interaction. Drug Metab Dispos, 2009; 37(8): 1658–1666. [PubMed: 19406954].
38. Cory Kalvass J, Maurer TS. Influence of nonspecific brain and plasma binding on CNS exposure: implications for rational drug discovery. Biopharm Drug Dispos, 2002; 23(8): 327–338. [PubMed: 12415573]
39. Jones DR, Gorski JC, Hamman MA, Mayhew BS, Rider S, Hall SD. Diltiazem inhibition of cytochrome P-450 3A activity is due to metabolite intermediate complex formation. J Pharmacol Exp Ther, 1999; 290(3): 1116–1125. [PubMed: 10454485]
40. Lindstrom TD, Hanssen BR, Wrighton SA. Cytochrome P- 450 complex formation by dirithromycin and other macrolides in rat and human livers. Antimicrob Agents Chemother, 1993; 37(2): 265–269. [PubMed: 8452357].
41. Wang Y-H, Jones DR, Hall SD. Prediction of cytochrome P450 3A inhibition by verapamil enantiomers and their metabolites. Drug Metab Dispos, 2004; 32(2): 259–266. [PubMed: 14744949].
42. Ma B, Prueksaritanont T, Lin JH. Drug interactions with calcium channel blockers: possible involvement of metabolite- intermediate complexation with CYP3A. Drug Metab Dispos, 2000; 28(2): 125–130. [PubMed: 10640508].
43. Zhao P, Lee CA, Kunze KL. Sequential metabolism is responsible for diltiazem-induced timedependent loss of CYP3A. Drug metabolism and disposition, 2007; 35(5): 704–712. [PubMed: 17293381].
44. Zhang X, Jones DR, Hall SD. Prediction of the effect of erythromycin, diltiazem, and their metabolites, alone and in combination, on CYP3A4 inhibition. Drug Metab Dispos, 2009; 37(1): 150–160. [PubMed: 18854379].
45. Nagar S, Korzekwa K. Drug Distribution. Part 1. Models to Predict Membrane Partitioning. Pharm Res, 2017; 34(3): 535–543. [PubMed: 27981450].
46. Cleland W. Partition analysis and concept of net rate constants as tools in enzyme kinetics. Biochemistry, 1975; 14(14): 3220–3224. [PubMed: 1148201].
47. Akaike H. A new look at the statistical model identification. IEEE Trans Autom Control, 1974; 19(6): 716–723.
48. Renwick AB, Watts PS, Edwards RJ, Barton PT, Guyonnet I, Price RJ, Tredger JM,

Pelkonen O, Boobis AR, Lake BG. Differential maintenance of cytochrome P450 enzymes in cultured precision- cut human liver slices. Drug Metab Dispos, 2000; 28(10): 1202–1209. [PubMed: 10997941].

49. Greenblatt DJ, Moltke LL, Harmatz JS, Chen G, Weemhoff JL, Jen C, Kelley CJ, LeDuc BW, Zinny MA. Time course of recovery of cytochrome p450 3A function after single doses of grapefruit juice. Clin Pharmacol Ther, 2003; 74(2): 121–129. [PubMed: 12891222].
50. Obach RS, Walsky RL, Venkatakrishnan K. Mechanism based inactivation of human cytochrome P450 enzymes and the prediction of drug-drug interactions. Drug Metab Dispos, 2006; 35: 246–255. [PubMed: 17093004].
51. Gibaldi, M., Perrier, D. Pharmacokinetics. 2nd. Vol. 15. Marcel Dekker; New York: 1982. Drugs and the Pharmaceutical Sciences
52. Vitro Metabolism- and Transporter-Mediated Drug-Drug Interaction Studies: Guidance for Industry. U.S. Department of Health and Human Services, Food and Drug Administration, Center for Drug Evaluation and Research (CDER); Silver Spring, MD: 2017. Available at https: // www.fda.gov/downloads/Drugs/GuidanceComplianceRegulatoryInformation/Guidances/ UCM581965.pdf.
53. Takahashi RH, Shahidi-Latham SK, Wong S, Chang JH. Applying Stable Isotope Labeled Amino Acids in Micropatterned Hepatocyte Coculture to Directly Determine the Degradation Rate Constant for CYP3A4. Drug Metab Dispos, 2017; 45(6): 581–585. [PubMed: 28289057].
54. Yang J, Liao M, Shou M, Jamei M, Yeo KR, Tucker GT, Rostami-Hodjegan A. Cytochrome p450 turnover: regulation of synthesis and degradation, methods for determining rates, and implications for the prediction of drug interactions. Curr Drug Metab, 2008; 9(5): 384–393. [PubMed: 18537575].
55. Pichard L, Fabre I, Daujat M, Domergue J, Joyeux H, Maurel P. Effect of corticosteroids on the expression of cytochromes P450 and on cyclosporin A oxidase activity in primary cultures of human hepatocytes. Mol Pharmacol, 1992; 41(6): 1047–1055. [PubMed: 1614409].
56. von Bahr C, Steiner E, Koike Y, Gabrielsson J. Time course of enzyme induction in humans: effect of pentobarbital on nortriptyline metabolism. Clin Pharmacol Ther, 1998; 64(1): 18–26. [PubMed: 9695715]
57. Chan CY, Roberts O, Hassan N, Lippert N, Siccardi M, Almond L, Owen A. Use of

mRNA suppression to estimate CYP3A4 protein degradation rate constant in primary human hepatocytes.Drug Metab Pharmacokinet, 2017; 32(1): S109.

58. Fromm MF, Busse D, Kroemer HK, Eichelbaum M. Differential induction of prehepatic and hepatic metabolism of verapamil by rifampin. Hepatology, 1996; 24(4): 796–801. [PubMed: 8855178].
59. Agrawal V, Choi JH, Giacomini KM, Miller WL. Substrate- specific modulation of CYP3A4 activity by genetic variants of cytochrome P450 oxidoreductase (POR). Pharmacogenet Genomics, 2010; 20(10): 611. [PubMed: 20697309].
60. Ekroos M, Sjogren T. Structural basis for ligand promiscuity in cytochrome P450 3A4. Proc NatlAcad Sci U S A, 2006; 103(37): 13682–13687. [PubMed: 16954191].
61. Shen L, Fitz off JF, Cook CS. Differential enantioselectivity and product-dependent activation and inhibition in metabolism of verapamil by human CYP3As. Drug Metab Dispos, 2004; 32(2): 186– 196. [PubMed: 14744940].
62. Berry LM, Zhao Z, Lin M-HJ. Dynamic modelling of cytochrome P450 inhibition in vitro: impact of inhibitor depletion on IC50-shift. Drug Metab Dispos, 2013; 41: 1433–1441. [PubMed: 23649703].
63. Peters SA, Schroeder P, Geri N, Dolgos H. Evaluation of the use of static and dynamic models to predict drug-drug interaction and its associated variability: impact on drug discovery and early development. Drug Metab Dispos, 2012; 40: 1495–1507. [PubMed: 22566536].
64. Vieira ML, Kirby B, Ragueneau-Majlessi I, Galetin A, Chien J, Einolf H, Fahmi O, Fischer V, Fretland A, Grime K, et al. Evaluation of various static in vitro–in vivo extrapolation models for risk assessment of the CYP3A inhibition potential of an investigational drug. Clin Pharmacol Ther, 2014; 95(2): 189–198. [PubMed: 24048277]
65. Fahmi OA, Maurer TS, Kish M, Cardenas E, Boldt S, Nettleton D. A combined model for predicting CYP3A4 clinical net drug-drug interaction based on CYP3A4 inhibition, inactivation, and induction determined in vitro. Drug Metab Dispos, 2008; 36(8): 1698–1708. [PubMed: 18490437]
66. Ramsden D, Zhou J, Tweedie DJ. Determination of a degradation constant for CYP3A4 by direct suppression of mRNA in a novel human hepatocyte model, HepatoPac. Drug Metab Dispos, 2015; 43(9): 1307–1315. [PubMed: 26076693]
67. Rostami-Hodjegan A, Wolff K, Hay AW, Raistrick D, Calvert R, Tucker GT. Population pharmacokinetics of methadone in opiate users: Characterization of time-dependent changes. Br JClin Pharmacol, 1999; 48(1): 43–52. [PubMed: 10383559]

68. Hsu A, Granneman GR, Witt G, Locke C, Denison J, Molla A, Valdes J, Smith J, Erdman K, Lyons N, et al. Multiple- dose pharmacokinetics of ritonavir in human immunodeficiency virus- infected subjects. Antimicrob Agents Chemother, 1997; 41(5): 898–905. [PubMed: 9145841]
69. Mao J, Mohutsky MA, Harrelson JP, Wrighton SA, Hall SD. Prediction of CYP3A mediated drug- drug interactions using human hepatocytes suspended in human plasma. Drug Metab Dispos, 2011; 39: 591–602. [PubMed: 21212240]
70. Vieira ML, Zhao P, Berglund E, Reynolds K, Zhang L, Lesko L, Huang SM. Predicting Drug Interaction Potential With a Physiologically Based Pharmacokinetic Model: A Case Study of Telithromycin, a Time-Dependent CYP3A Inhibitor. Clin Pharmacol Ther, 2012; 91(4): 700–708.[PubMed: 22398966]
71. Galetin A, Burt H, Gibbons L, Houston JB. Prediction of time-dependent CYP3A4 drug-drug interactions: impact of enzyme degradation, parallel elimination pathways, and intestinal inhibition. Drug Metab Dispos, 2006; 34(1): 166–175. [PubMed: 16221752]
72. Yeo KR, Jamei M, Yang J, Tucker GT, Rostami-Hodjegan A. Physiologically based mechanistic modelling to predict complex drug–drug interactions involving simultaneous competitive and time- dependent enzyme inhibition by parent compound and its metabolite in both liver and gut—the effect of diltiazem on the time-course of exposure to triazolam. Eur J Pharm Sci, 2010; 39(5): 298–309. [PubMed: 20025966]
73. Quinney SK, Zhang X, Lucksiri A, Gorski JC, Li L, Hall SD. Physiologically based pharmacokinetic model of mechanism-based inhibition of CYP3A by clarithromycin. Drug Metab Dispos, 2010; 38(2): 241–248. [PubMed: 19884323]
74. Zhang X, Quinney SK, Gorski JC, Jones DR, Hall SD. Semi physiologically based pharmacokinetic models for the inhibition of midazolam clearance by diltiazem and its major metabolite. Drug MetabDispos, 2009; 37(8): 1587–1597. [PubMed: 19420129]
75. Nagar S, Tucker J, Weiskircher EA, Biopath S, Hidalgo IJ, Korzekwa K. Compartmental models for apical efflux by P- glycoprotein—part 1: evaluation of model complexity. Pharm Res, 2014; 31(2): 347–359. [PubMed: 24019023].
76. Kulkarni P, Korzekwa K, Nagar S. Intracellular unbound atorvastatin concentrations in the presence of metabolism and transport. J Pharmacol Exp Ther, 2016; 359: 26–36. [PubMed: 27451408]
77. Jansat JM, Costa J, Salvà P, Fernandez FJ, Martinez-Tobed A. Absolute bioavailability, pharmacokinetics, and urinary excretion of the novel antimigraine agent almotriptan in healthy male volunteers. J Clin Pharmacol, 2002; 42(12): 1303–1310. [PubMed:

12463724].

78. McEnroe JD, Fleishaker JC. Clinical pharmacokinetics of almotriptan, a serotonin 5-HT 1B/1D receptor agonist for the treatment of migraine. Clin Pharmacokinet, 2005; 44(3): 237–246. [PubMed: 15762767].
79. McEwen J, Salva M, Jansat J, Cabarrocas X. Pharmacokinetics and safety of oral almotriptan in healthy male volunteers. Bio pharm Drug Dispos, 2004; 25(7): 303–311. [PubMed: 15386481].
80. AXERT (almotriptan malate) Tablets Prescribing Information; 10071702. U.S. Food and Drug Administration; Silver Spring, MD: 2007. Available at https: //www.accessdata.fda.gov/ drugsatfda_docs/label/2009/021001s008s009lbl.pdf.
81. Brown HS, Galetin A, Halifax D, Houston JB. Prediction of in vivo drug-drug interactions from in vitro data: factors affecting prototypic drug-drug interactions involving CYP2C9, CYP2D6 and CYP3A4. Clin Pharmacokinet, 2006; 45(10): 1035–50. [PubMed: 16984215]
82. Yang J, Jamei M, Yeo KR, Tucker GT, Rostami-Hodjegan A. Prediction of intestinal first-pass drugmetabolism. Curr Drug Metab, 2007; 8(7): 676–684. [PubMed: 17979655]
83. Varma MV, Orbach RS, Rotter C, Miller HR, Chang G, Steyn SJ, El-Kattan A, Troutman MD. Physicochemical space for optimum oral bioavailability: contribution of human intestinal absorption and first-pass elimination. J Med Chem, 2010; 53(3): 1098–1108. [PubMed: 20070106]
84. Engel G, Hofmann U, Heidemann H, Cosme J, Eichelbaum M. Antipyrine as a probe for human oxidative drug metabolism: Identification of the cytochrome P450 enzymes catalyzing 4- hydroxyantipyrine, 3-hydroxymethylantipyrine, and norantipyrine formation. Clin Pharmacol Ther,1996; 59(6): 613–623. [PubMed: 8681486]
85. Sharer JE, Wrighton SA. Identification of the human hepatic cytochromes P450 involved in the in vitro oxidation of antipyrine. Drug Metab Dispos, 1996; 24(4): 487–494. [PubMed: 8801065].
86. Danhof M, Van Zuilen A, Boeijinga J, Breimer D. Studies of the different metabolic pathways of antipyrine in man. Eur J Clin Pharmacol, 1982; 21(5): 433–441. [PubMed: 7075648].
87. Kirch W, Görg K. Clinical pharmacokinetics of atenolol—a review. Eur J Drug Metab Pharmacokinet, 1982; 7(2): 81–91. [PubMed: 6749509]
88. Wander GS, Chhabra ST, Kaur K. Atenolol Drug Profile. J Assoc Physicians India, 2009; 57: 13–16. [PubMed: 19753752].

89. Gertz M, Harrison A, Houston JB, Galetin A. Prediction of human intestinal first-pass metabolism of 25 CYP3A substrates from in vitro clearance and permeability data. Drug Metab Dispos, 2010; 38(7): 1147–1158. [PubMed: 20368326].
90. Louie, SW., Shou, M. Drug-Metabolizing Enzymes, Transporters, and Drug–Drug Interactions. In: Lee, MS., Zhu, M., editors. Mass Spectrometry in Drug Metabolism and Disposition: Basic Principles and Applications. Wiley; Hoboken, NJ, 2011; 83-149.
91. Ohno Y, Hisaka A, Suzuki H. General framework for the quantitative prediction of CYP3A4- mediated oral drug interactions based on the AUC increase by Coad ministration of standard drugs. Clin Pharmacokinet, 2007; 46(8): 681–696. [PubMed: 17655375]
92. Galetin A, Gertz M, Houston JB. Contribution of intestinal cytochrome p450-mediated metabolism to drug-drug inhibition and induction interactions. Drug Metab Pharmacokinet, 2010; 25(1): 28–47. [PubMed: 20208387]
93. Shou M, Hayashi M, Pan Y, Xu Y, Morrissey K, Xu L, Skiles GL. Modelling, prediction, and in vitro in vivo correlation of CYP3A4 induction. Drug Metab Dispos, 2008; 36(11): 2355–2370. [PubMed: 18669588]
94. Gertz M, Davis JD, Harrison A, Houston JB, Galetin A. Grapefruit juice-drug interaction studies as a method to assess the extent of intestinal availability: utility and limitations. Curr Drug Metab, 2008; 9(8): 785–795. [PubMed: 18855612]
95. Stangier J, Stähle H, Rathjen K, Fuhr R. Pharmacokinetics and pharmacodynamics of the direct oral thrombin inhibitor dabigatran in healthy elderly subjects. Clin Pharmacokinet, 2008; 47(1): 47–59. [PubMed: 18076218]
96. Blech S, Ebner T, Ludwig-Schwellinger E, Stangier J, Roth W. The metabolism and disposition of the oral direct thrombin inhibitor, dabigatran, in humans. Drug Metab Dispos, 2008; 36: 386–399. [PubMed: 18006647]
97. Brown HS, Ito K, Galetin A, Houston JB. Prediction of in vivo drug–drug interactions from in vitro data: impact of incorporating parallel pathways of drug elimination and inhibitor absorption rate constant. Br J Clin Pharmacol, 2005; 60(5): 508–518. [PubMed: 16236041]
98. Lappin G, Shashikumar Y, Jochemsen R, Weaver RJ, Gesson C, Houston B, Oosterhuis B, Bjerrum OJ, Rowland M, Garner C. Pharmacokinetics of fexofenadine: evaluation of a microdose and assessment of absolute oral bioavailability. Eur J Pharm Sci, 2010; 40(2): 125–131. [PubMed: 20307657]
99. Hesse LM, Venkatakrishnan K, von Moltke LL, Shader RI, Greenblatt DJ. CYP3A4 is the

major CYP isoform mediating the in vitro hydroxylation and demethylation of flunitrazepam. Drug Metab Dispos, 2001; 29(2): 133–140. [PubMed: 11159802]

100. Drouet-Coassolo C, Iliadis A, Coassolo P, Antoni M, Cano J. Pharmacokinetics of flunitrazepam following single dose oral administration in liver disease patients compared with healthy volunteers. Fundam Clin Pharmacol, 1990; 4(6): 643–651. [PubMed: 2096104]
101. Dettli L. The kidney in pre-clinical and clinical pharmacokinetics. Rinsho Yakuri, 1984; 15(1): 241–254.
102. Xu L, Chen Y, Pan Y, Skiles GL, Shou M. Prediction of human drug-drug interactions from time-dependent inactivation of CYP3A4 in primary hepatocytes using a population-based simulator. Drug Metab Dispos, 2009; 37(12): 2330–2339. [PubMed: 19773538]
103. Cusack B, O'malley K, Lavan J, Noel J, Kelly J. Protein binding and disposition of lignocaine in the elderly. Eur J Clin Pharmacol, 1985; 29(3): 323–329. [PubMed: 4076329]
104. Bargetzi MJ, Aoyama T, Gonzalez FJ, Meyer UA. Lidocaine metabolism in human liver microsomes by cytochrome P450IIIA4. Clin Pharmacol Ther, 1989; 46(5): 521–527. [PubMed: 2582709]
105. Perucca E, Richens A. Reduction of oral bioavailability of lignocaine by induction of first pass metabolism in epileptic patients. British journal of clinical pharmacology, 1979; 8(1): 21–31. [PubMed: 552293]
106. Wang J-S, Backman JT, Taavitsainen P, Neuvonen PJ, Kivistö KT. Involvement of CYP1A2 and CYP3A4 in Lidocaine N- Deethylation and 3-Hydroxylation in Humans. Drug Metab Dispos, 2000; 28(8): 959–965. [PubMed: 10901707]
107. Beckett A, Boyes R, Appleton P. The metabolism and excretion of lignocaine in man. J Pharm Pharmacol, 1966; 18(S1): 76S–81S.
108. Isohanni, M. PhD Dissertation. University of Helsinki; Helsinki, Finland: 2009. Cytochrome P450-mediated drug interactions affecting lidocaine.